RESEARCH ARTICLE

Resistance reduction of patterned surface inspired by cuticle structure of *Achalinus spinalis*

Jiahui ZHAO[1], **Keju JI**[1,*], **Qin CHEN**[2], **Muhammad Niaz KHAN**[1], **Chongwen TU**[1], **Ze MA**[1], **Jianming WU**[1], **Jian CHEN**[1], **Zhendong DAI**[1,*]

[1] *Jiangsu Provincial Key Laboratory of Bionic Functional Materials, College of Mechanical and Electrical Engineering, Nanjing University of Aeronautics and Astronautics, Nanjing 210016, China*

[2] *Chengdu Institute of Biology, Chinese Academy of Sciences, Chengdu 610041, China*

© The author(s) 2022.

Abstract: The crawling process of snakes is known to have fascinating tribological phenomena, whereas investigations on their frictional properties depending on patterned cuticles are insufficient. In this study, we have designed and fabricated biomimetic microstructures inspired by the geometric microunits of *Achalinus spinalis* cuticle using polyurethane acrylate (PUA) material and performed its tribological analysis. The micro-morphology of this *Achalinus*-inspired textured polymer surface (AITPS) is characterized by the closely and evenly quasi-rectangular microgrooves, periodically arranged along certain orientations. We have compared the frictional performance of our fabricated AITPS with other competitive microstructure, using a smooth steel ball and commercial clay as an interacting surface. After performing massive friction tests with steel ball and clay, AITPS still maintains good resistance reduction performed compared to the patterned surface with straight microgrooves, which is most likely due to the reduction of actual contact areas at the frictional interface.

Keywords: biomimetic; microstructure; friction; resistance reduction

1 Introduction

The burrowing locomotion of organisms within granular solid terrestrial substrates (sand, soil, and muddy sediments) have attracted considerable attention because of their specific bionic inspiration. In general, organisms solve the problem of high frictional resistance and drag in subterranean environments that display both solid friction and viscous fluid-like behaviors. This is mainly achieved by two processes: optimizing locomotion and evolving tissues, especially cuticle structures.

For kinematics, many studies reported that the mechanical responses (viscosity, density, graininess, etc.) of medium determine behaviors of organisms. By observing the locomotion of sandfish lizards (*Scincus scincus*) under dry sand, Maladen et al. [1] found that the lizard no longer uses limbs to propel their body but creates forward motion by propagating an undulatory traveling wave down the body. Nevertheless, Baumgartner et al. [2] and Wu et al. [3] have confirmed that the micro or nanostructured surfaces of sandfish cuticle cannot reduce the frictional resistance from sand. On the other hand, physical structure of organisms plays a key role in subterranean locomotion. Tong et al. [4] reported that the embossed textured surfaces of dung beetles do not stick to dung or soil, which can reduce the adhesion and friction between cuticle surfaces and soil. Zhao et al. [5] introduced an earthworm-inspired texture structure on their designed

---

liquid-releasable polymer coatings, which shows good frictional performance for many cycles at a constant loading of 50 kPa. Lee et al. [6, 7] reported a porous lubricant-infused surface inspired by the mucus secretion and storage systems of loach, hagfish, and seaweed, which shows promising potential for frictional resistance reduction. However, the morphologies and behaviors of slender burrowing snakes living in cohesive moist soil are poorly understood.

Many groups have studied the frictional properties of snakes during crawling. Baum et al. [8] reported that the ventral scale of a snake can generate high friction for propulsion and low friction to slide, which can be accredited to the anisotropic structures of snake cuticle. Up to now, most studies mainly focused on the anisotropic frictional properties of the microstructure on snakes' ventral scale surface in contact with the ground [9–13]. Less literature has been reported on the subsurface resistance reduction mechanisms of burrowing snakes [14]. The methods and routes of the burrowing locomotion for snakes are flexibly adjusted according to the specific subsurface conditions [15]. For example, crawling along rocks and soil cracks; or burrowing through loose soil, mud, and humus. As they dig underground, burrowing snakes can promote their scales forward by driving all muscles of the whole body [16, 17]. In this process, their bodies are in direct and close contact with surrounding cohesive soil, which can make severe resistance. Therefore, deep studies of the resistance-reducing biological structure of burrowing snakes and the dry friction process, lacking in lubrication, are of great importance for understanding the evolution of biological resistance reduction.

In this study, we have explored the morphology of a typical burrowing snake, *Achalinus spinalis*, and observed the grid-like microstructures built with closely and evenly quasi-rectangular microgroove arrays on their cuticle. Using picosecond laser processing equipment and microstructure replication technology, a variety of patterned surfaces with different morphologies were fabricated. Their friction properties are tested under different conditions using a universal mechanical tester. Finally, the obtained results were analyzed to reveal the frictional behavior of the patterned surface on *Achalinus spinalis* cuticle for burrowing in the subsurface locomotion.

2 Experimental

2.1 Animals

The first investigation of *Achalinus spinalis* was reported by Huang et al. [15]. This fossorial snake, belonging to the Xenodermatidae family, is widely distributed in China, Japan, and Northern Vietnam. In natural environments, *Achalinus spinalis* is a nocturnal, secretive, and subterranean snake, relying mainly on earthworm, and is usually hidden in deciduous and humic layers of earth, close to the streams and ditches [16]. In this study, animal specimens were obtained from Chengdu Institute of Biology, Chinese Academy of Sciences, China. The macro and micro-morphologies of snake cuticle were observed by the super resolution digital microscope (VHX-2000, KEYENCE, Japan), scanning electron microscope (SEM; ZEISS ΣIGMA, Germany), and atomic force microscope (AFM; Dimension ICON, Bruker, Germany).

As shown in Fig. 1(a), the dark–brown scales of *Achalinus spinalis* show iridescent colors and metallic luster under light, which can be attributed to structural colors [15]. The whole body of *Achalinus spinalis* is covered with regularly arranged scales, whose sizes are mainly characterized in millimeter-scale. The detailed images of snake scales were visualized by the super resolution digital microscope (VHX-2000, KEYENCE, Japan) with a dual-light high-magnification zooming lens (Figs. 1(b) and 1(c)). Compared with the ventral scale of other colubrid snakes, *Achalinus spinalis* shows a wider size and can be observed on both sides. Their anisotropic ventral scales exhibit an asymmetric arrangement on the longitudinal axis of the snake body, while their tilted tips pointed towards the rear direction. Driving through these anisotropic ventral scales, the contraction of the snake body can promote them forward and change their scales from laying individuals to overlapping one another, which is instrumental in burrowing and hunting [16]. The micro-morphologies of snake cuticle from different body parts were investigated by the SEM images at an acceleration voltage of 8 kV (Figs. 1(d)–1(g)). Before the visualization of texture, snake cuticle was fixed on a collar pad and sputter-coated with a gold–palladium layer. The high-magnification image by the SEM (Fig. 1(d)) reveals that the dorsal scale has a
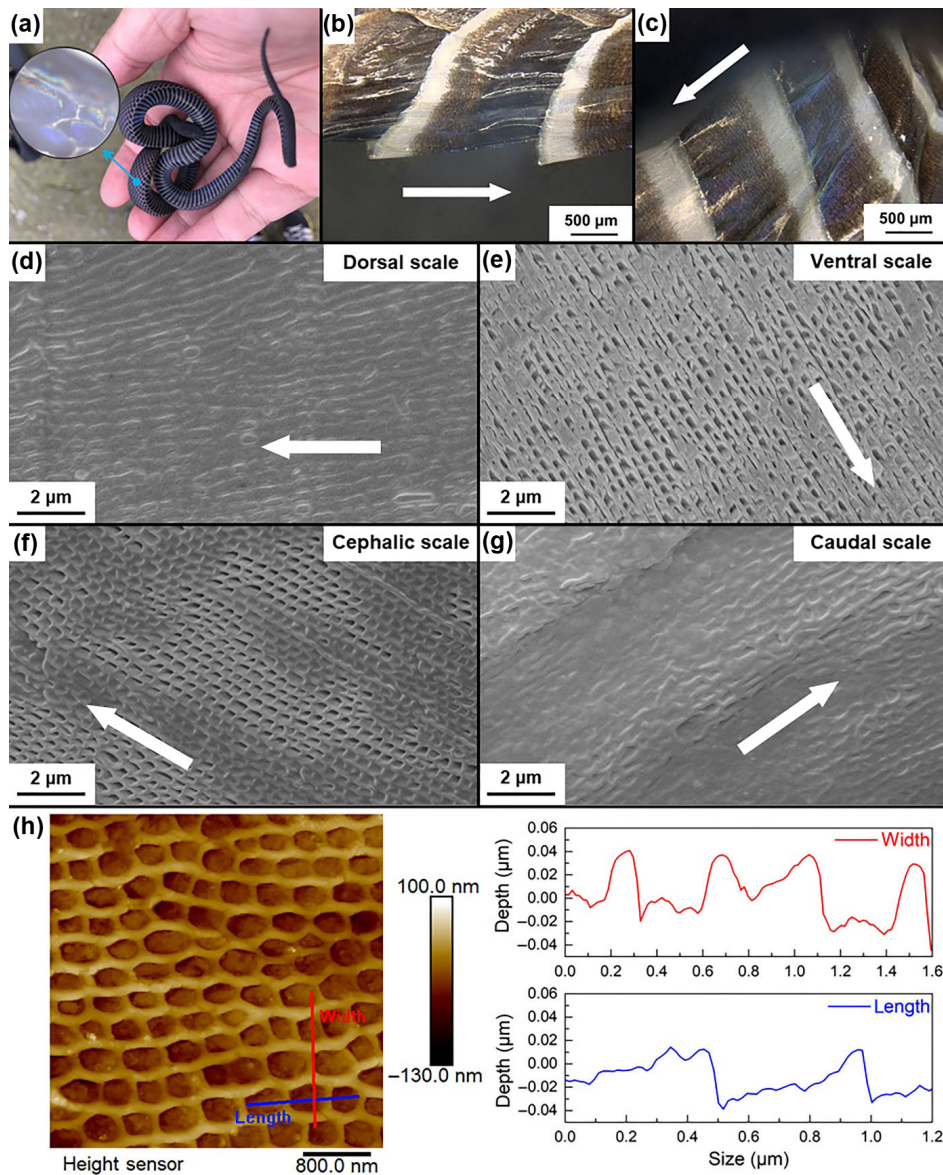
Fig. 1 (a) Structural color of *Achalinus spinalis* cuticle; (b, c) microscopic images of ventral scale for *Achalinus spinalis*; (d–g) SEM images of dorsal scale, ventral scale, cephalic scale, and caudal scale for *Achalinus spinalis*; and (h) AFM images of *Achalinus spinalis* cuticle and the width, length, and depth profiles along the corresponding lines.

grid-like microstructures arranged with closely and periodically quasi-rectangular microgrooves. For comparison, the micro-morphologies of the ventral scale, cephalic scale, and caudal scale were captured, as shown in Figs. 1(e)–1(g). It is shown that each snake scale of *Achalinus spinalis* has a similar surface morphology with an approximate size. The grid-like microstructure is composed of massive regular furrows, which are parallel to the longitudinal axis of the snake cuticle. Inner arrows indicate the overall pointing directions of furrows at different scale of snake surfaces.

In further observations, these furrows are formed by series of microgrooves, which are extended along the certain crawling direction of snake movement and staggered with those of left and right sides. To determine the more precise parameters of the snake cuticle microstructure, the analysis of surface profiles is performed using the AFM, as shown in Fig. 1(h). The AFM images broadly confirmed the morphological findings observed by the SEM. These closely and evenly arrayed microgrooves are mainly 0.53±0.08 μm long and 0.32±0.04 μm in width, which is almost half
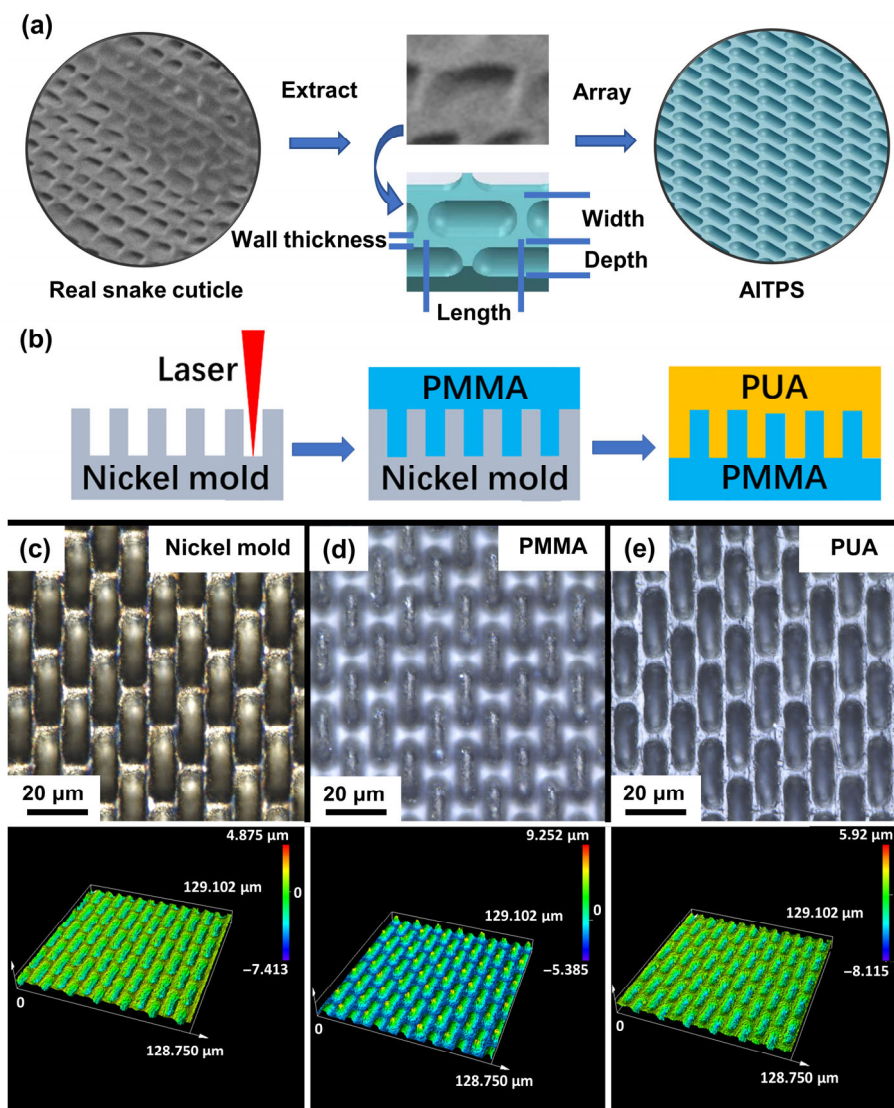
Fig. 2 (a) Schematic description of characteristic (width, length, depth, and wall thickness) extraction of real snake cuticle on biomimetic surface; (b) detailed manufacturing process of picosecond laser manufacturing and two-step replica molding technique; and (c–e) LEXT images of nickel positive mold, polymethyl methacrylate negative mold, and AITPS. Note: PMMA is the abbreviation of polymethyl methacrylate.

to length of grooves. The depth of microgrooves distributed in the range of 0.05–0.06 μm. Most notably, the observed average thickness of the grid-like microstructure is about 0.15±0.05 μm. Such geometric parameters of microstructure on snake cuticle have been rarely reported in Refs. [8–19]. Furthermore, considering the living environment of *Achalinus spinalis*, this kind of grid-like microstructure with well-arranged arrays of microgrooves may be favorable for reducing the resistance between snake cuticle and soil, which can enhance the dynamic performance underground.

2.2 Design and preparation of patterned surfaces

Based on the key morphological observation from the above SEM and AFM images, *Achalinus*-inspired textured polymer surface (AITPS) was fabricated by a picosecond laser manufacturing and a two-step replica molding technique. Firstly, the periodically patterned nickel molds were fabricated by a commercially available Nd:YVO4 picosecond pulse laser system (PX100-2-GF-z, EdgeWave GmbH, Germany). The system can deliver 12-ps pulses at a central wavelength of 532 nm with a pulse energy of up to 100 μJ (repetition

rate = 250 kHz). An *x*–*y* motorized translation stage was used for sample positioning and translation. The depth and line width of microstructures can be controlled within a limited range by regulating some parameters such as laser output power, processing speed, processing time, and pulse rate. The line width can be controlled down to 5 μm when the processable power is minimized. As the laser output power increases, the line width can be widened and reaches a maximum value of about 20 μm. Secondly, replication of the microstructures was performed by using a two-step moulding technique. In the first step, the fabricated patterned surfaces on the master nickel mold were replicated by polymethyl methacrylate sheets by a thermal nanoimprinting apparatus to obtain a negative mold. In the second step, the negative mold was casted with a prepolymer of polyurethane acrylate (PUA; SC2565, M220, and M2101, Miwon Specialty Chemical; Darocur 1173, Ciba Specialty Chemical), which polymerizes within 60 s under ultraviolet light. The elastic modulus of the polymerized PUA is about 10 MPa, which is similar to that of a snake cuticle [8, 20]. As a typical example, the detailed manufacturing process of AITPS is shown in Figs. 2(a) and 2(b). The as-prepared patterned surfaces were observed by means of a three dimensional (3D) laser confocal microscope (LEXT OLS5000, OLYMPUS, Japan). The geometric parameters of fabricated microgrooves are characterized by 25.5±0.5 μm in length, 10.1±0.1 μm in width, and 4.9 μm as an average depth (Figs. 2(c)–2(e)). The average thickness of its grid-like microstructure is about 4.5±0.5 μm. Such a geometric implementation of the patterned PUA surface, similar to the biological microstructures of *Achalinus spinalis* cuticle, enabled us to a standardized and comparable investigation of the influence of the patterned surface on the tribological properties.

2.3 Frictional measurements

The frictional parameters were measured using an UMT (UMT-2, Bruker, Germany) with a sensor range of 0–5,000 mN. The friction coefficients (μ) were defined according to the Amontons' friction law: $\mu = F_t/F_n$ (F_t: tangential force; F_n: normal force) [12]. The typical measurement procedures are demonstrated in Fig. 3, where the green arrows indicate the movement direction of tribometer. In this case, the relative parallel movement between sensor and the substrate was regulated by the angled table (Fig. 3(a); SA07A-RT, KOHZU, Japan). As an interacting surface, a smooth steel ball (3 mm diameter) and commercial clay were chosen as tribometers. The steel ball was used to simulate the friction properties between snake cuticle and smooth cobble surface (Fig. 3(b)). The commercial clay was used to simulate the actual frictional conditions to testing samples, as experienced to snake cuticles by moist soil and soil (Fig. 3(c)). To confirm the resistance reduction effect of biomimetic microstructures, the length of the fabricated patterned surface was limited in the middle of samples for the friction tests. The tribometer passes through three parts in sequence: smooth PUA surface, patterned surface (AITPS), and smooth PUA surface.
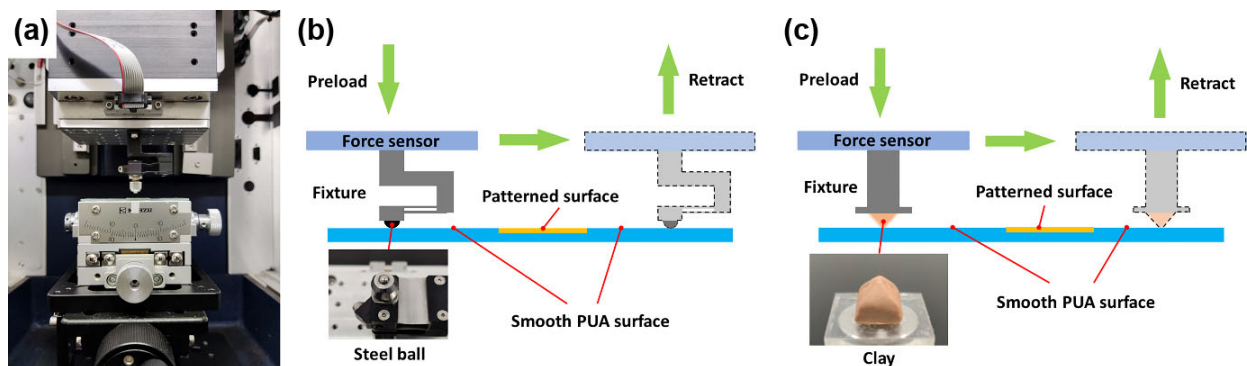

Fig. 3 (a) Optical image of the test platform and the relative parallel movement regulated by the angled table (SA07A-RT, KOHZU, Japan); (b, c) schematic illustration of frictional measurement procedures with smooth steel ball and commercial clay, respectively, where the size of the patterned surface was limited in the middle of samples, and the green arrows indicate the movement direction of tribometer.

3 Results and discussion

3.1 Frictional properties

In order to characterize the frictional behavior of AITPS, friction tests were performed using smooth steel ball and commercial clay to measure the F_t and F_n. Figures 4(a)–4(d) represent the frictional force–time curves of the as-prepared samples with different preloads (500, 1,000, 1,500, and 2,000 mN) and different sliding speeds (1.0, 1.5, 2.0, 2.5, and 3.0 mm/s). When the tribometer comes into contact with the smooth surface, all the curves fluctuate around fundamental frictional-force values at the corresponding preloads despite the speed variations. While, when the steel ball contact with AITPS, the values of frictional force decreased significantly and rapidly. Thus, the AITPS demonstrated a considerable reduction of the frictional resistance compared to the same polymer with the smooth surface. As shown in Fig. 4(e), the friction coefficients of AITPS decreased from 0.25 to 0.15 with nearly identical values for different preload conditions with a sliding speed of 1.0 mm/s. Using clay tribometer as the interacting surface, continuous measurements were performed more than 10 times for the sample along the longitudinal directions to obtain stable friction coefficients. As shown in Fig. 4(f), the friction

coefficients of AITPS decreased from 0.8 to 0.6, which illustrates the significance of their resistance reduction properties. These friction characteristics illustrate a stable resistance reduction effect of the as-prepared AITPS samples without showing viscoelasticity [21].

For comparative analysis, two additional patterned surfaces, which have been reported by many researchers [22–27], were prepared by laser manufacturing with the same technological parameters, as used for AITPS (Fig. 5(a)). The sample with consecutive and straight microgrooves, as shown in Fig. 5(b), is referred as Structure-B, which has been reported to exhibit good drag reduction in liquids [24]. The sample with a similar microstructure as that of AITPS but with a wider distance between microgrooves, as shown in Fig. 5(c), is referred as Structure-C, which was introduced to compare with AITPS in order to investigate the effect of wall thickness on friction reduction properties. Measurements were performed with steel ball along the longitudinal (Fig. 5(d)) and lateral (Fig. 5(e)) directions of the microgrooves on samples. For every sample, there is almost no visible difference in the resistance reduction effect measured along these two different directions. In comparison (Figs. 5(f) and 5(g)), the minimum friction coefficient of Structure-C is much higher than those of AITPS and Structure-B, which shows a poor resistance
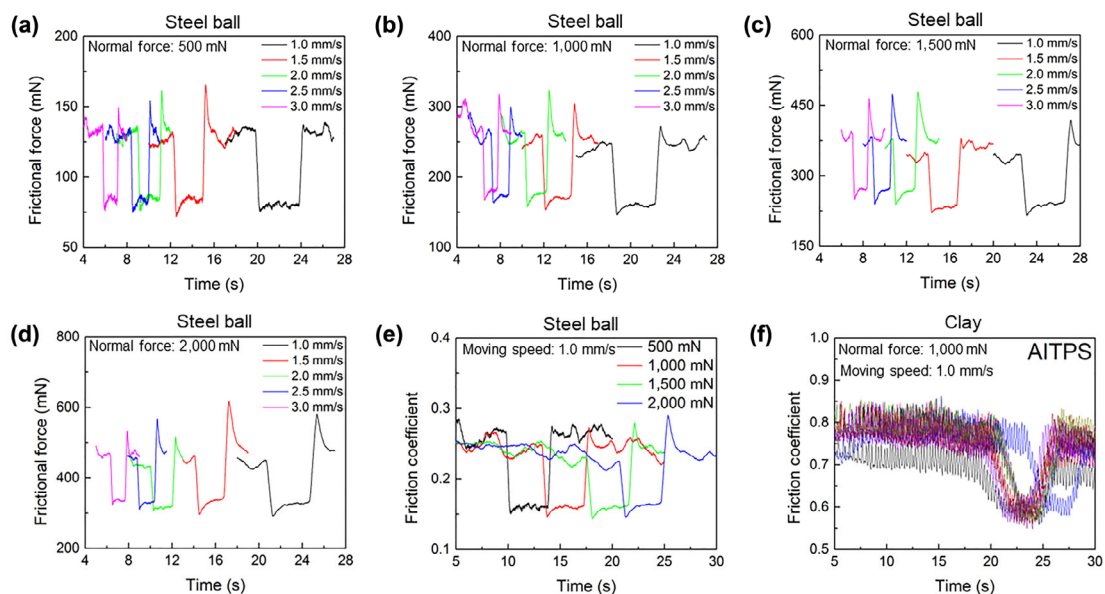

Fig. 4 Testing with smooth steel ball: (a–d) force–time curves of AITPS with different preloads (500, 1,000, 1,500, and 2,000 mN) and different sliding speeds (1.0, 1.5, 2.0, 2.5, and 3.0 mm/s); (e) friction coefficients of AITPS for different preloads with a moving speed of 1.0 mm/s. Testing with commercial clay: (f) friction coefficient curves of AITPS after 10 times of measurements.
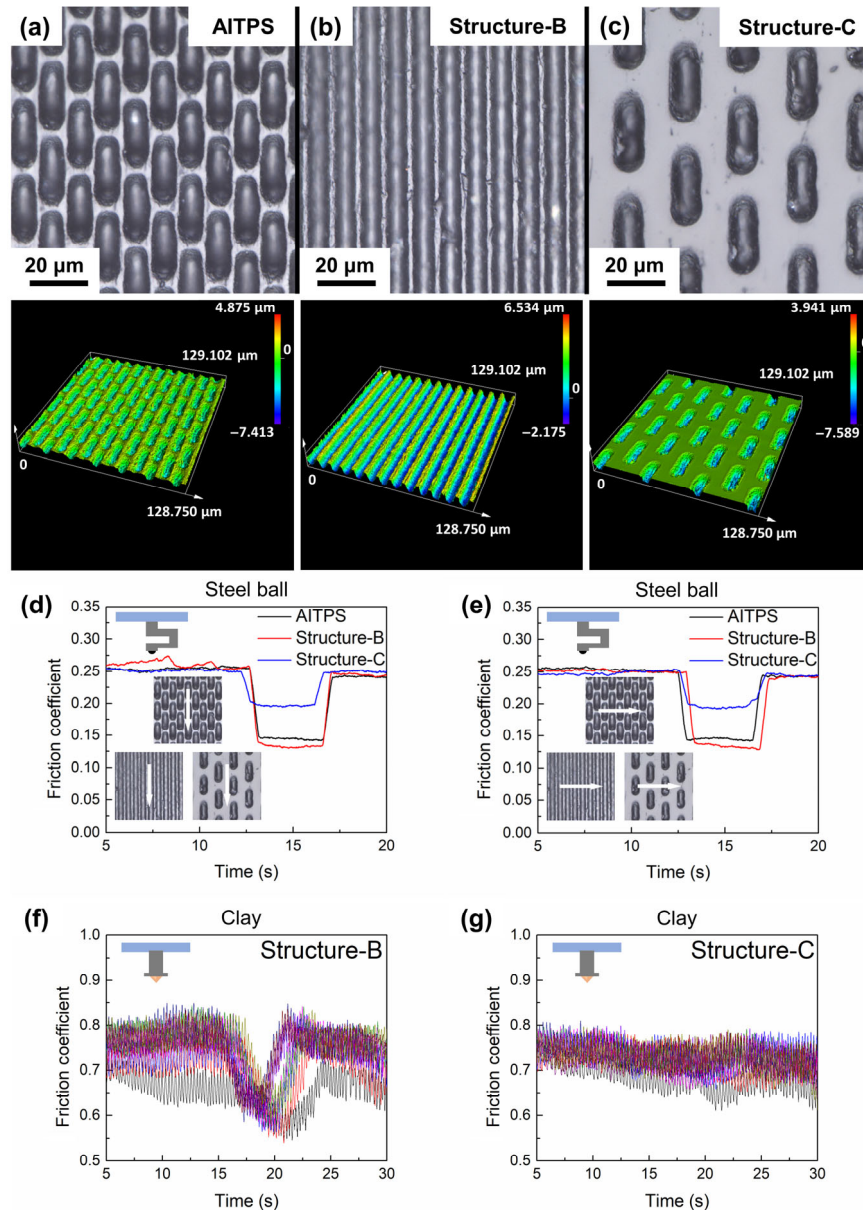
Fig. 5 (a–c) LEXT images of AITPS, Structure-B, and Structure-C; (d, e) friction coefficient curves of three patterned surfaces in longitudinal and lateral directions in contact with smooth steel ball, respectively; and (f, g) friction coefficient curves of Structure-B and Structure-C after 10 times of measurements in contact with commercial clay, respectively.

reduction property of Structure-C. The friction coefficient of Structure-B without partition is slightly lower than that of AITPS. For the contact pair with the clay tribometer, the friction performance of Structure-B is similar with that of AITPS. While, comparatively, Structure-C almost lost its resistance reduction performance. The experimental results and Refs. [23–26] indicate that smaller actual contact areas of the patterned surfaces resulted in a smaller friction coefficient under the same testing conditions.

3.2 Resistance reduction mechanism

In order to make the explanation of resistance reduction mechanism of AITPS more convincing, the effect of depth (Fig. 6) and width and length (Fig. 7) on the frictional properties of AITPS were added to investigate.

Frictional measurements performed with both smooth steel ball (Fig. 6(e)) and clay tribometer (Fig. 6(f)) showed that when the depth of the
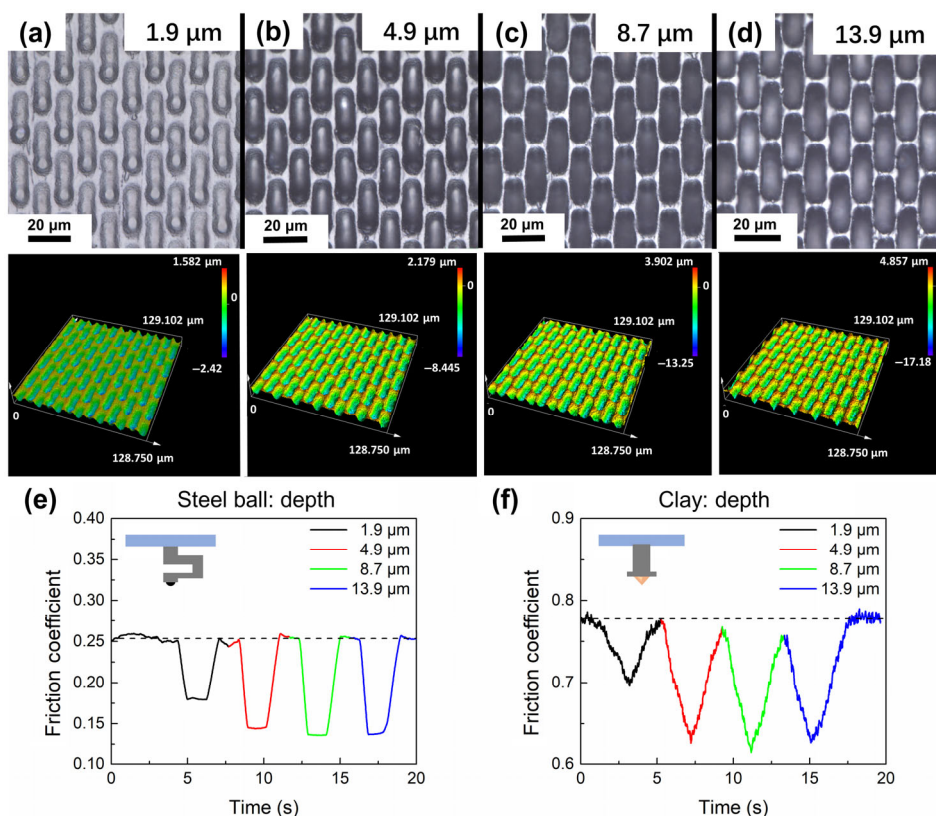
Fig. 6 (a–d) LEXT images of AITPS with the depth of microgrooves increased in different degrees (1.9, 4.9, 8.7, and 13.9 μm); (e, f) frictional measurement results of AITPS with different depths in contact with steel ball and commercial clay, respectively, with the minimum value of the friction coefficients tended to reduce first and then became stable.

microgrooves increased in different degrees (1.9, 4.9, 8.7, and 13.9 μm), the minimum value of the friction coefficients tended to reduce first and then became stable. The change took place when the depth to width ratios of microgrooves increased to 1: 2. For polymeric elastomer, there is a positive correlation between frictional coefficient and actual contact area at the interface [10]. When the microgroove depth is shallow, the top surface of grid-like microstructure has a rounded shape and larger actual contact areas. As the depth of microgrooves increase, the top shape of grid-like microstructure becomes sharp, making the actual contact areas reduced. However, increasing the depth of the microgrooves cannot infinitely reduce the actual contact areas. The results reconfirmed that the minimum friction coefficient is positively correlated with the actual contact area, keeping the width and length of AITPS microgrooves constant.

Figure 7 illustrates the effect of microgroove sizes on friction properties. The as-prepared AITPS with designed sizes (width × length) of 5.8 μm × 12.6 μm,

10.2 μm × 26.8 μm, and 20.5 μm × 56.9 μm were referred as AITPS-S, AITPS-M, and AITPS-L, respectively. While the depth to width ratios of microgrooves for all of these samples were kept 1: 2. For the contact pair with the smooth steel ball (Fig. 7(d)), the minimum friction coefficient of AITPS-M is slightly lower than that of AITPS-S and is almost approximate to that of AITPS-L. As a comparison, almost similar resistance reduction properties of AITPS-S and AITPS-M, as well as the poor resistance reduction performance of AITPS-L revealed that smaller size of AITPS microstructure has better resistance reduction performance in contact with clay (Fig. 7(e)). Due to the fluidity of clay, when clay comes in contact with the surface of AITPS, it has the tendency to enter the microgroove. For the AITPS with smaller microstructure sizes, the pressure of the clay in contact with the AITPS can be more evenly dispersed by the grid-like microstructure, which can slow down the tendency for clay to enter the microgrooves.
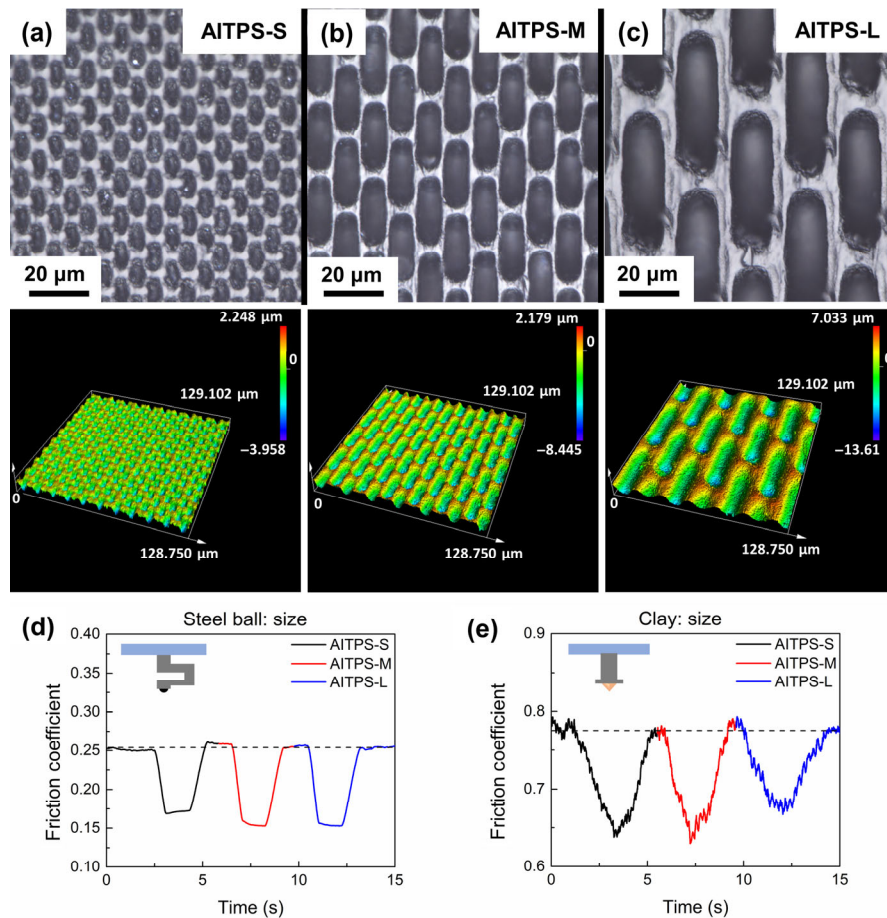
As shown in Figs. 8(a) and 8(b), frictional

Fig. 7 (a–c) LEXT images of AITPS with designed sizes (width × length) of 5.8 μm × 12.6 μm, 10.2 μm × 26.8 μm, and 20.5 μm × 56.9 μm; (d, e) frictional measurement results of AITPS with different sizes in contact with steel ball and commercial clay, respectively, showing a better resistance reduction performance of AITPS with a smaller microstructure size.

measurements with a clay tribometer were performed 100 times for both AITPS and Structure-B, and the microscopic images after the 0th, 10th, 30th, and 100th times are given. The microgrooves of AITPS still have unfilled sections even after 100 times of tests. However, the straight furrows of Structure-B were almost filled after 30 times of tests. After 100 times of performing friction tests with viscoelastic clay, smooth PUA surface exhibit irregular friction coefficient curves at relatively faster measuring speeds (more than 1.0 mm/s) [21]. Meanwhile, friction coefficient curves of AITPS and Structure-B show entirely contrary results. The friction coefficient curves of AITPS still shows impressive resistance reduction results for all testing speeds in this study (Fig. 8(c)). However, the friction coefficient curves of Structure-B in Fig. 8(d) indicate the three convex peaks at different testing speeds, which show an abnormal resistance

enhancement phenomenon.

This frictional behavior could be attributed to the low fluidity and high viscosity of the semi-fluid clay. For polymeric elastomer, there was a positive correlation between friction coefficient and actual area at the contact interface [10]. When the clay moves with normal preload on such a filled surface, the clay with high viscosity inside the straight furrows of Structure-B will be carried along with it, which resulted in the increased contact area and consequently leads to the increase in resistance. In comparison, the quasi-rectangular microgrooves of AITPS are only partially filled. The resistance reduction behavior of AITPS can be expressed by two mechanisms. On the one hand, the partitions of grid-like microstructure most likely support the contacted clay, which can reduce actual contact areas. On the other hand, the quasi-rectangular microgrooves of AITPS are capable
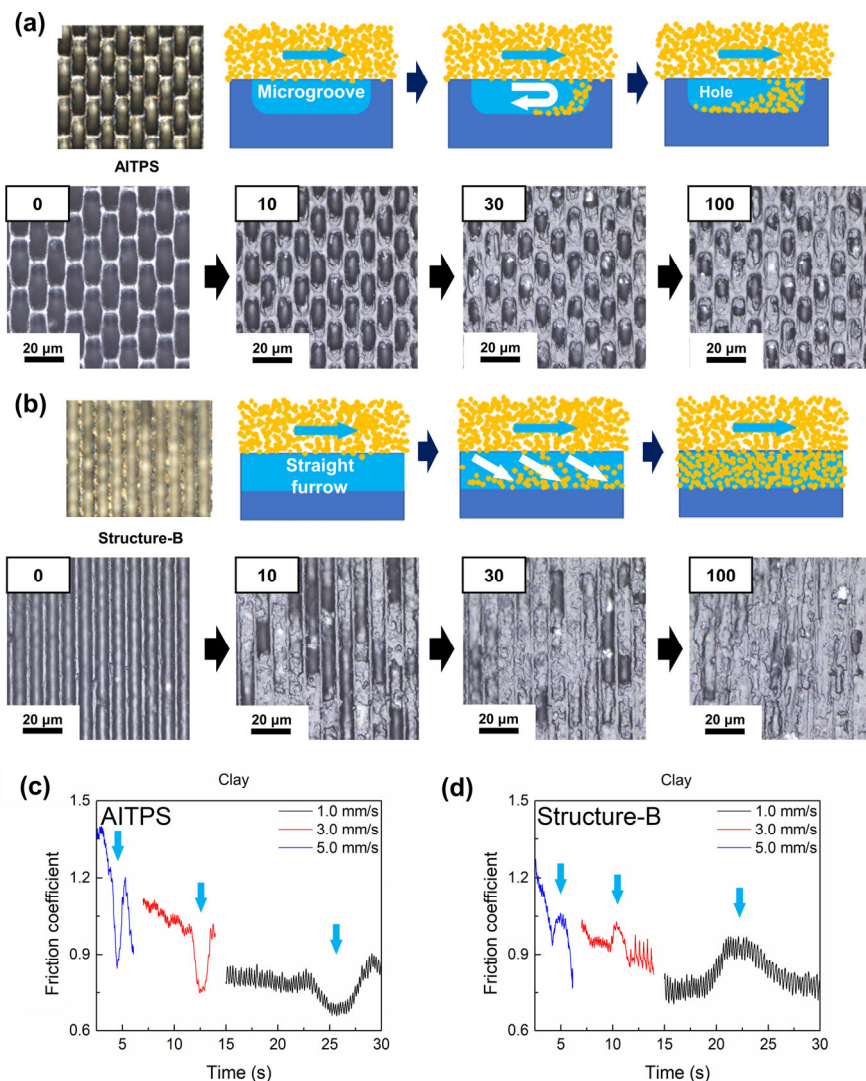
Fig. 8 Resistance reduction mechanisms: (a, b) schematic illustrations and microscopic images of AITPS and Structure-B after 0th, 10th, 30th, and 100th times of measurements, respectively; (c, d) friction coefficient curves of AITPS and Structure-B after 100th tests at different measuring speeds (1.0, 3.0, and 5.0 mm/s), respectively.

of holding and segmenting the filled clay particles, which can reduce their moving distance and create unfilled holes. In this process, due to the high viscosity of clay, empty cavities will be formed at the back of microgrooves, which can reduce the actual contact areas at the interface. The surfaces morphologies of AITPS and Structure-B before and after 100 dynamic friction tests using clay tribometer are shown in the video in the Electronic Supplementary Material (ESM).

4 Conclusions

The *Achalinus spinalis* cuticle demonstrated a regular matrix structure with massive quasi-rectangular microgrooves along with the crawling direction. Biomimetic patterned polymer surface inspired by *Achalinus spinalis* cuticle was designed and fabricated by picosecond pulse laser engraving technology combined with a two-step replicating technique. Frictional force evaluation indicated an excellent resistance reduction performance of biomimetic AITPS. The post-experiment images of tested samples revealed the two mechanisms for resistance reduction of biomimetic AITPS: (1) The partitions of grid-like microstructure can support the contacted clay, which can reduce actual contact areas. (2) Microgrooves can tolerate and segment the microparticles in the

semi-fluid clay, which can reduce the moving distance of clay particles inside the microgrooves.

Acknowledgements

Electronic Supplementary Material Supplementary material is available in the online version of this article at https://doi.org/10.1007/s40544-022-0694-6.

References

[1] Maladen R D, Ding Y, Li C, Goldman D I. Undulatory swimming in sand: Subsurface locomotion of the sandfish lizard. *Science* **325**(5938): 314–318 (2009)

[2] Baumgartner W, Saxe F, Weth A, Hajas D, Sigumonrong D, Emmerlich J, Singheiser M, Böhme W, Schneider J M. The sandfish's skin: Morphology, chemistry and reconstruction. *J Bionic Eng* **4**(1): 1–9 (2007)

[3] Wu W B, Lutz C, Mersch S, Thelen R, Greiner C, Gomard G, Hölscher H. Characterization of the microscopic tribological properties of sandfish (*Scincus scincus*) scales by atomic force microscopy. *Beilstein J Nanotechnol* **9**: 2618–2627 (2018)

[4] Tong J, Sun J Y, Chen D H, Zhang S J. Geometrical features and wettability of dung beetles and potential biomimetic engineering applications in tillage implements. *Soil Till Res* **80**(1–2): 1–12 (2005)

[5] Zhao H X, Sun Q Q, Deng X, Cui J X. Earthworm-inspired rough polymer coatings with self-replenishing lubrication for adaptive friction-reduction and antifouling surfaces. *Adv Mater* **30**(29): 1802141 (2018)

[6] Lee S J, Kim H N, Choi W, Yoon G Y, Seo E. A nature-inspired lubricant-infused surface for sustainable drag reduction. *Soft Matter* **15**(42): 8459–8467 (2019)

[7] Seo E, Park J, Gil J E, Lim H, Lee D, Lee S J. Multifunctional biopolymer coatings inspired by loach skin. *Prog Org Coat* **158**: 106383 (2021)

[8] Baum M J, Kovalev A E, Michels J, Gorb S N. Anisotropic friction of the ventral scales in the snake *Lampropeltis getula californiae*. *Tribol Lett* **54**(2): 139–150 (2014)

[9] Wu W B, Yu S D, Schreiber P, Dollmann A, Lutz C, Gomard G, Greiner C, Hölscher H. Variation of the frictional anisotropy on ventral scales of snakes caused by nanoscale steps. *Bioinspir Biomim* **15**(5): 056014 (2020)

[10] Ren Y L, Zhang L, Xie G X, Li Z B, Chen H, Gong H J, Xu W H, Guo D, Luo J B. A review on tribology of polymer composite coatings. *Friction* **9**(3): 429–470 (2021)

[11] Filippov A E, Westhoff G, Kovalev A, Gorb S N. Numerical model of the slithering snake locomotion based on the friction anisotropy of the ventral skin. *Tribol Lett* **66**(3): 119 (2018)

[12] Baum M J, Heepe L, Fadeeva E, Gorb S N. Dry friction of microstructured polymer surfaces inspired by snake skin. *Beilstein J Nanotechnol* **5**: 1091–1103 (2014)

[13] Zheng L, Zhong Y H, Gao Y H, Li J Y, Zhang Z H, Liu Z N, Ren L Q. Coupling effect of morphology and mechanical properties contributes to the tribological behaviors of snake scales. *J Bionic Eng* **15**(3): 481–493 (2018)

[14] Meng Y G, Xu J, Jin Z M, Prakash B, Hu Y Z. A review of recent advances in tribology. *Friction* **8**(2): 221–300 (2020)

[15] Huang R Y, Peng L F, Yu L, Huang T Q, Jiang K, Ding L, Chang J K, Yang D C, Xu Y H, Huang S. A new species of the genus *Achalinus* from Huangshan, Anhui, China (Squamata: Xenodermidae). *Asian Herpetol Res* **12**(2): 178–187(2021)

[16] Yamasaki Y, Mori Y. Seasonal activity pattern of a nocturnal fossorial snake, *Achalinus spinalis* (Serpentes: Xenodermidae). *Curr Herpetol* **36**(1): 28–36 (2017)

[17] Van der Kooij J, Povel D. Scale sensillae of the file snake (*Serpentes*:*Acrochordidae*) and some other aquatic and burrowing snakes. *Neth J Zool* **47**(4): 443–456 (1996)

[18] Zhao Y Z, Su Y L, Hou X Y, Hong M H. Directional sliding of water: Biomimetic snake scale surfaces. *Opto-Electron Adv* **4**(4): 210008 (2021)

[19] Hoge A R, Santos P S. Submicroscopic structure of "stratum corneum" of snakes. *Science* **118**(3067): 410–411 (1953)

[20] Yi H, Hwang I, Lee J H, Lee D, Lim H, Tahk D, Sung M, Bae W G, Choi S J, Kwak M K, et al. Continuous and scalable fabrication of bioinspired dry adhesives via a roll-to-roll process with modulated ultraviolet-curable resin. *ACS Appl Mater Inter* **6**(16): 14590–14599 (2014)

[21] Zimm B H. Dynamics of polymer molecules in dilute solution: Viscoelasticity, flow birefringence and dielectric loss. *J Chem Phys* **24**(2): 269–278 (1956)

[22] Xing Y Q, Deng J X, Feng X T, Yu S. Effect of laser surface texturing on Si_3N_4/TiC ceramic sliding against steel under dry friction. *Mater Design* **52**: 234–245 (2013)

[23] Pettersson U, Jacobson S. Friction and wear properties of micro textured DLC coated surfaces in boundary lubricated sliding. *Tribol Lett* **17**(3): 553–559 (2004)

[24] Xiao G J, Zhang Y D, He Y, He S. Optimization of belt grinding stepover for biomimetic micro-riblets surface on titanium alloy blades. *Int J Adv Manuf Technol* **110**(5–6): 1503–1513 (2020)

[25] Pang K, Wang D Z. Study on the performances of the drilling process of nickel-based superalloy Inconel 718 with differently micro-textured drilling tools. *Int J Mech Sci* **180**: 105658 (2020)

[26] Hamilton D B, Walowit J A, Allen C M. A theory of lubrication by microirregularities. *J Basic Eng* **88**(1): 177–185 (1966)

[27] Costa H L, Schille J, Rosenkranz A. Tailored surface textures to increase friction—A review. *Friction* **10**(9): 1285–1304 (2022)

Jiahui ZHAO. He received his B.E. and M.E. degrees from School of Materials Science and Engineering, China University of Mining and Technology. He is currently perusing a Ph.D. degree from Nanjing University of Aeronautics and Astronautics (NUAA), China. His interested research areas include bionics, tribology, and micro/nano manufacturing technology.

Keju JI. He obtained his Ph.D. degree in 2016 from College of Mechanical and Electrical Engineering, NUAA, China. Now, he is an associate professor in NUAA and the vice director at Jiangsu Provincial Key Laboratory of Bionic Functional Materials, China. He is a committee member of the Council of Chinese Mechanical Engineering in Tribology. He has successively presided and participated in many research projects and has published more than 30 papers and gotten more than 10 patents. And his research interests include the precision manufacturing technology, bionic adhesive materials, and bionic surface and interface.

Zhendong DAI. He obtained his Ph.D. degree in 1999 from College of Mechanical and Electrical Engineering, NUAA, China. He is one of the Chinese delegates of International Institute of Bionic Engineering, an executive member of the Council of Chinese Mechanical Engineering in Tribology, and a member of the Academic Committee, State Key Laboratory of Solid Lubrication, China. He is also the member of editorial board of many journals such as *Journal of Bionic Engineering*, *International Journal of Vehicle Autonomous System*, *Tribology*. His research areas include bionics, light material, control of bionics, bio-robots, and biological robots. He has successively presided and participated in many research projects and has published more than 200 papers and gotten more than 20 patents.